NPL
National Physical Laboratory

NPL REPORT ENG 59

Preliminary investigation into the use of a network-based technique for calibration of 3D laser scanners

Hughes, B, Ferrucci, M, Forbes, A

NOVEMBER 2015

National
Measurement
System

Preliminary investigation into the use of a network-based technique for the calibration of 3D laser scanners

Ben Hughes, Massimilliano Ferrucci, Alistair Forbes
Engineering Measurement Division
Operations Directorate

ISSN 1754-2987

National Physical Laboratory
Hampton Road, Teddington, Middlesex, TW11 0LW

Approved on behalf of NPLML by Dr Andrew Lewis, Science Area Leader, Dimensional Metrology

CONTENTS

1 INTRODUCTION

Three dimensional (3D) laser scanners have been employed for some years in applications such as cultural heritage, forensics, 3D land (topography) and "as built" surveying. Three dimensional laser scanners use a high-speed laser-based range finder mounted on a rapidly rotating head to scan the environment, thus producing a high-density digital point cloud representation of the scene that can be archived and analysed as required. Often, full colour information is recorded simultaneously by a coaxially mounted camera to provide a more realistic 3D image.

In recent years, the range measurement capability of laser scanners has been improved to the extent that sub-millimetre accuracy and range noise can be achieved over tens of metres or more. In fact the National Institute of Standards and Technology (NIST) in the US has recently reported the development of a 3D scanner with a 10 μm precision at a range of 10.5 m[1]. This increase in accuracy together with the increased requirement for rapid acquisition of high-quality data at relatively low cost in high-value manufacturing industries, and applications such as reverse engineering and factory maintenance has led to the migration of three dimensional laser scanners from surveying to engineering application.

With the increase in take-up of 3D laser scanner technology and the ever higher accuracy demands, comes increased demand for calibration, performance verification and measurement traceability. These issues of calibration and traceability for non-contact optical measurement systems are complex and not simply limited to the calibration and compensation of systematic errors in the instrument itself. Significant systematic errors can arise due to, for example, the interaction between the scanning laser light and the material and surface properties of the objects being scanned, and the incident angle of the laser beam to the surface. However, for the class of 3D laser scanner considered in this work, the level of range accuracy is such that the accuracy is dominated by the geometrical errors of the instrument and the accuracy of the laser ranging system.

Calibration of a laser ranging system is relatively straight forward and can be carried out using, for example a calibrated length artefact or a more accurate coordinate measurement system such as a laser tracker, or by comparison with a reference interferometer. However, there is no documentary standard covering the calibration or performance verification of laser scanners. Furthermore, volumetric performance tests conducted at NIST have shown that systematic errors can still be evident after calibration and that they can be attributed to incomplete compensation for geometrical alignment errors[2, 3]. There is, therefore, a need to improve the way that these devices are calibrated in order to realise their full potential.

The National Physical Laboratory (NPL) has therefore carried out an initial investigation into the feasibility of calibration of the geometric errors of 3D scanners using the "network method" - previously developed at NPL for laser tracker calibration[4, 5].

In section 2 of this report, we briefly describe a mathematical model of the geometric errors of a laser scanner. In section 3, we provide a summary of the network method used for calibration of instrument errors. In section 4 we present the method used for testing a laser scanner. The results and observation are presented in section 5, with a final summary and conclusions in section 6.

2 GEOMETRIC ERROR MODEL OF A LASER SCANNER

An idealised representation of the internal geometry of a laser scanner is shown in Figure 1. A rotating platform mounted on a fixed base carries a laser source and rotating mirror assembly; the platform rotates about the standing axis, *Z*. The laser source is aligned such that the laser beam is aligned coaxially with the rotation axis of the rotating mirror, known as the transit axis, *T*. The laser beam reflects off the rotating mirror at the point, *O*, which lies at the point of intersection of the mirror surface and the rotation axes, *T* and *Z*. The mirror is tilted at 45° with respect to the axis *T* such that the laser beam reflects off it to a point, *P,* on the *NZ* plane where *ON* is perpendicular to *OT*.

Angle encoders measure the rotation angles, *Hm* of the spinning platform around the *Z* axis, and *Vm* of the rotating mirror assembly around the *T* axis. It is assumed that these encoders are perfectly aligned with the rotation axes and are free from other errors. The angles measured by the encoders, together with the range information, *Rm*, obtained from the laser ranger provide point coordinates in spherical polar form.

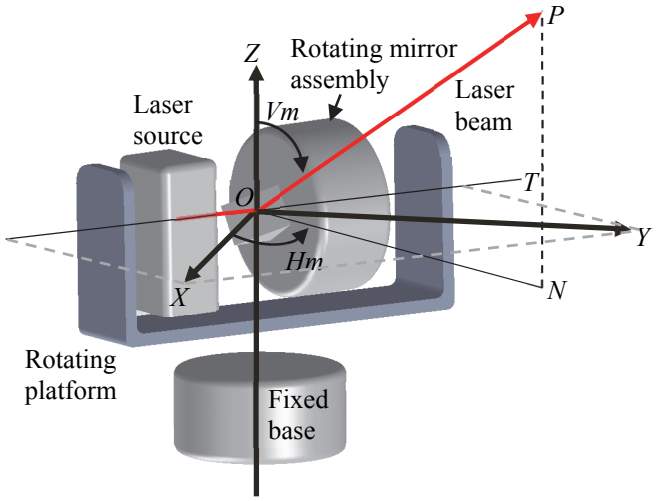

Figure 1 The ideal geometry of a laser scanner.

Deviations in the perfect geometry described above lead to systematic errors in the range and angle data and hence errors in the coordinate measurements. These geometric errors need to be compensated to obtain the best performance from the scanner. A method is, therefore, required to determine the geometrical errors.

A geometric error model of a typical laser scanner has been developed by NIST[6, 7, 8]. The eighteen parameter model is:

$$\Delta Rm = k\big(x_2\, sin(Vm)\big) + x_{10}$$

$$\Delta Hm = k\left[\frac{x_{1z}}{Rm\, tan(Vm)} - \frac{x_3}{Rm\, sin(Vm)} + \frac{x_{5z}}{tan(Vm)} - \frac{x_6}{\sin(Vm)} + \frac{x_7}{tan(Vm)} + x_{8x}cos(Hm) + x_{8y}sin(Hm)\right] + \left[\frac{x_{1n}}{Rm} + x_{5n} + x_{11a}\, cos(2\, Hm) + x_{11b}\sin(2\, Hm)\right]$$

$$\Delta Vm = k\left[\frac{x_{1n}cos(Vm)}{Rm} + \frac{x_2 cos(Vm)}{Rm} + x_4 + x_{5n}cos(Vm) - x_{9n}cos(Vm)\right] + \left[\frac{-x_{1z}cos(Vm)}{Rm} - x_{5z}cos(Vm) + x_{9z}cos(Vm) + x_{12a}cos(2\, Vm) + x_{12b}cos(2\, Vm)\right]$$

Where *ΔRm*, *ΔHm* and *ΔVm* are the errors in range, azimuth and elevation respectively, the parameter *k* is 1 for points measured in *front-face* (when the point is in front of the scanner) and -1 for points measured in *back-face* (when the point is behind the scanner). The model parameters are as described in Table 1.

Table 1 The eighteen parameters of the NIST error model

Parameter	Description
x_{1n}	Beam offset along N
x_{1z}	Beam offset along Z
x_2	Transit axis offset
x_3	Mirror offset
x_4	Vertical index offset
x_{5n}	Beam tilt along N
x_{5z}	Beam tilt along Z
x_6	Mirror tilt
x_7	Transit axis tilt
x_{8x}	Horizontal encoder eccentricity along X
x_{8y}	Horizontal encoder eccentricity along Y
x_{9n}	Vertical encoder eccentricity along N
x_{9z}	Vertical encoder eccentricity along Z
x_{10}	Range zero offset
x_{11a}	Horizontal encoder scale error (second order)
x_{11b}	Horizontal encoder scale error (second order)
x_{12a}	Vertical encoder scale error (second order)
x_{12b}	Vertical encoder scale error (second order)

In [7] the twelve parameters that are sensitive to *two-face* tests (tests involving points measured in front-face and in back-face) were determined by fitting the model parameters to data obtained from a series of two-face tests on a reference artefact. In this work, we fit all eighteen parameters to our data, as described below.

3 THE NETWORK METHOD FOR INSTRUMENT CALIBRATION

The network method of instrument calibration can be thought of as a generalisation of the bundle adjustment used in photogrammetry. Bundle adjustment refers to fitting the parameters of a mathematical model of the measurement system to the data obtained. In photogrammetry, the model includes parameters that describe the *exterior orientation* – the position and orientation of the camera(s), and the *interior orientation* – the errors in the camera system. Photogrammetry is a triangulation technique that uses only angle data.

The generalised method used for the work reported here applies to instruments that have sensors providing any combination of angle and range data. The method involves:

- establishing a mathematical model of the systematic errors of the instrument under test;
- measuring the apparent position of multiple targets using the instrument under test from multiple (at least four) different locations;
- fitting the parameters of a model of the experiment to the observed range and angle data, where the model of the experiment includes parameters that describe:
    - the instrument position and orientation,
    - the target positions,
    - the geometrical errors of the instrument under test; and
- computing the uncertainties associated with the model parameters obtained.

For a detailed explanation of the mathematics involved in this method as applied to laser tracker calibration see [4, 5].

4 METHOD

The scanner used for the experiments reported was a Surphaser model 25HSX IR-X scanner with the following specifications:

- range: 0.3 m – 30 m;
- range noise (1 sigma, 90 % Lambertian surface): 0.1 mm at 3 m range;
- range uncertainty at 5 m with contrast target: 0.5 mm.

The targets were 1.5 inch tooling balls mounted in magnetic nests fixed to columns, floor, bench and other solid structures within the laboratory. A total of twenty six targets were used spread over a volume of approximately 4.9 m × 6.7 m × 3.8 m. The balls were spray coated with titanium dioxide powder to ensure a matt surface more suited to detection by the scanner.

Compensation for geometric errors was turned off in the scanner software by editing the error compensation file and setting the compensation parameters to zero.

The following scan settings were used:

- configuration: 1 pass HQ;
- horizontal resolution: 40 LPD (lines per degree);
- vertical resolution: 40 PPD (points per degree).

The scene was scanned from four locations using SurphExpress software (version 2.50). Each scan covered an azimuth range of 359° (the maximum allowed by the software), so that all target spheres were scanned in front-face and back-face. Obtaining data in front-face and back-face maximises the sensitivity of the experiment to the geometric errors as twelve of the eighteen parameters change sign between front-face and back-face. Each scan was manually edited to exclude data points that were not on or near the sphere targets.

Figure 2 Example data set after manual editing. Only data on or near the target spheres remains.

Figure 2 shows an example of a typical scan after removing points not on or near the target spheres. The resulting point clouds were then exported and processed to do the following.

1. Separate points that lie on the spheres into those scanned in front-face and those in back-face.
2. Identify the data points that lie on each sphere.
3. Fit points identified in step 2 to a sphere to locate sphere centres.
4. Use sphere centres with network software to determine locations of target spheres, scanner positions and orientations and geometric errors, and uncertainties in all these parameters.

Bespoke software written in LabVIEW 2013 and Matlab R2014a was used to process the experimental data. A brief summary of the processing follows.

4.1 SEPARATE POINTS INTO FRONT-FACE AND BACK-FACE

The exported data was in the form of a comma separated variable (CSV) file of *x, y, z* coordinates. This data was first converted to spherical polar form. An example of the un-processed angle data is shown in the plot of Figure 3. The discontinuities in the data correspond to the edges of each region of data in the point cloud.

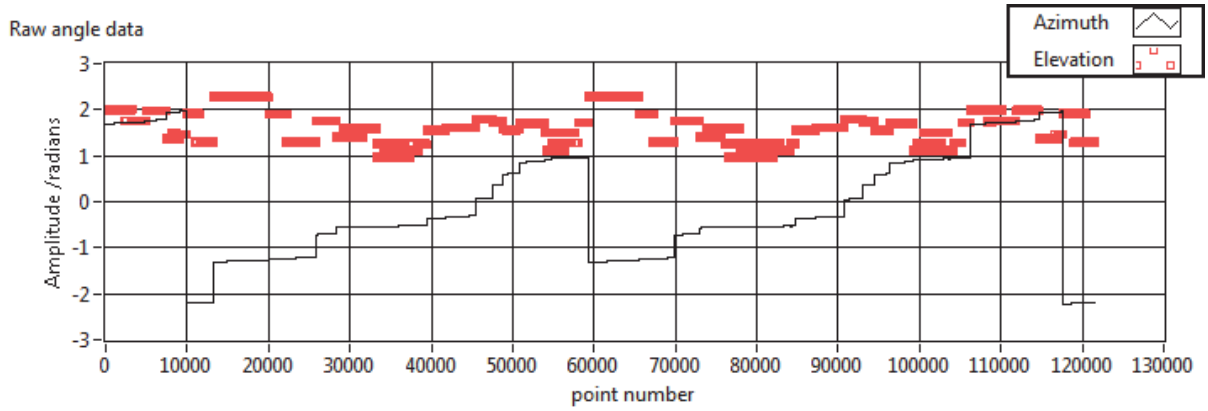

Figure 3 An example of typical un-processed angle data.

The data file is arranged such that data obtained in front-face occupies approximately the first half of the data, with the back-face data occupying the remainder of the file. In the data set shown in Figure 2, the break between front-face and back-face data clearly comes just before point number 60000 as indicated by the large decrease in the azimuth data.

Another indicator of the transition from front-face to back-face data in the file is the change in scan direction in elevation; for front-face points, the scan direction is down, whereas for back-face points the scan direction is up. To reliably locate the point index in the data file where the transition from front-face to back-face occurred, we differentiated the angle data and scanned the differentiated data for a spike in the elevation accompanied by a change in sign of the elevation data.

Figure 4 shows a close up view of the region of the differentiated angle data where the transition from front-face to back-face occurs. This is clearly indicated by a spike in the differentiated azimuth data with a corresponding change in sign from negative to positive in the differentiated elevation data.

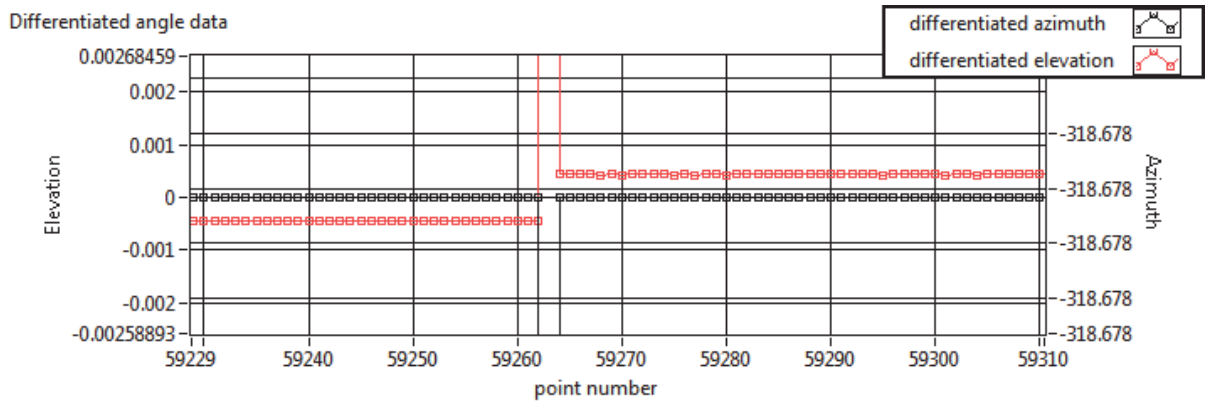

Figure 4 Close up view of the region of the differentiated angle data showing the location where the transition from front-face to back-face occurs - at point number 59263.

The data file was then split into two parts each containing either front-face or back-face data only and each part processed to locate an approximate position of the sphere centres. An example of a point cloud dataset after splitting into front-face and back-face data is shown in Figure 5.

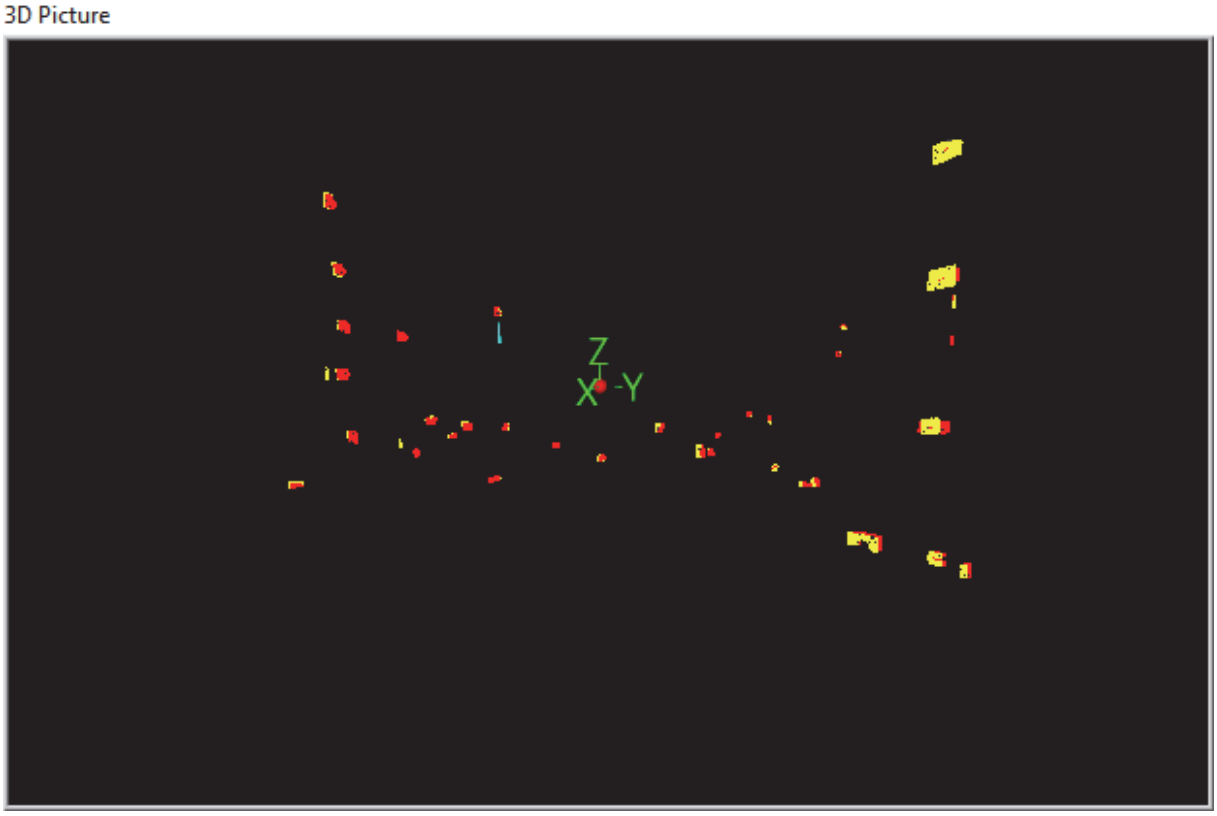

Figure 5 An example of a point cloud after splitting into points scanned in front-face (red) and back-face (yellow).

4.2 IDENTIFY DATA POINTS THAT LIE ON EACH SPHERE

After splitting the point cloud into two data sets containing either points scanned in front-face or points scanned in back-face, a 3D variant of the Hough transform algorithm was developed to process the data sets to identify the data points that lie on each of the target spheres. A *kd*-tree data structure was constructed to make searching the data more efficient. The algorithm works as follows:

1. For each point, P_i, in the point cloud:
   Find the nearest neighbours and form a surface around P_i.
   Find the surface normal at P_i.
   Generate two points, A_{i+} and A_{i-}, a distance R along the normal on either side P_i (where R is the nominal radius of the sphere).

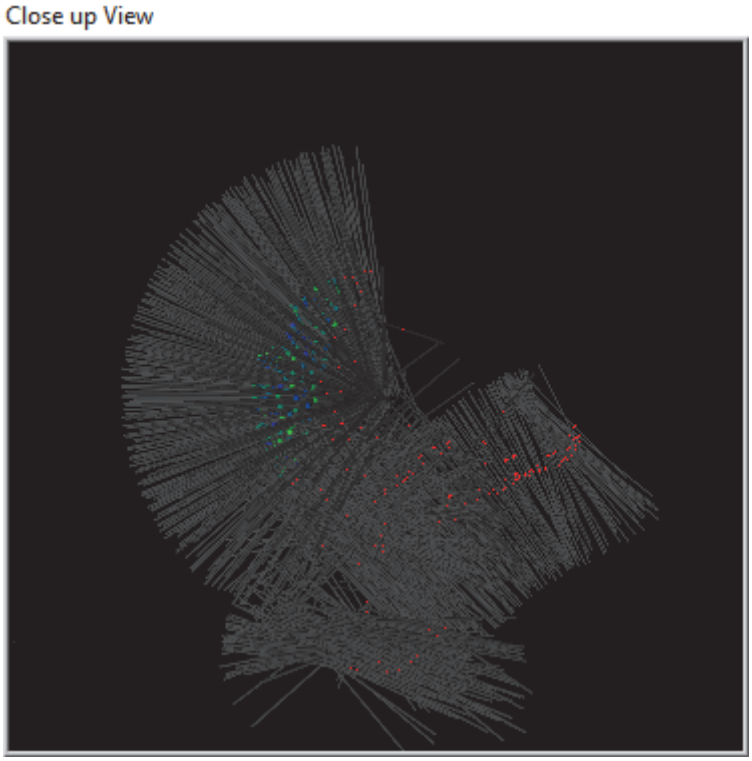

Figure 6 The output of Step 1. Points near a target sphere with their normal vectors drawn in grey a length *R* on either side of the surface at that point.

2. Form a 3D accumulator vector, ACC*(x, y, z, count)*, with a *x, y, z* coordinate resolution of 10 mm, with each *count* element initialised to zero.

3. For each point, A_{i+} and A_{i-}:
   Increment the *count* element in ACC that has *x, y, z* coordinates nearest to the point A_{i+}, A_{i-}.

4. For each element in ACC with $count \neq 0$:
   If the *count* in ACC > *threshold* then add the *x, y, z* coordinates in ACC to a list of nominal target centres, *Cnom*.

5. For each nominal target centre in *Cnom*:
   Find the points, $SP_{j,k}$, in the point cloud within $R \pm r$ of *Cnom*, where r is a radial tolerance, j is the target index, $1 \leq j \leq N_t$, where N_t is the number of target spheres and k is the point index for the j^{th} target, $1 \leq k \leq M_j$, where M_j is the number of points on the j^{th} target sphere.

The output of Step 1 of the algorithm is shown graphically in Figure 6, which shows the computed normal vectors (grey) through some of the points in the point cloud around one of the targets. Each normal vector is drawn with a length of 2R and centred on the individual point. The ends of the normal vectors therefore represent the points A_{i+} and A_{i-}. The vectors through the points that are on the target sphere all point to a common centre. These points were identified as being on the sphere by the algorithm and are coloured green/blue in the image. The points that were not found to be on the sphere are coloured

red. Figure 7 shows two examples of sections of the data sets around a target. Each target appears twice in the image; once in data points scanned in front-face and once from data points scanned in back-face.

4.3 FIT POINTS TO A SPHERE

Once the points on each target sphere, $SP_{*,k}$, had been identified, they were used to compute the approximate coordinates of each sphere centre using a standard library routine within LabVIEW (NI_gmath.lvlib:Fitting on a Sphere.vi), which computes the centre coordinates and radius of the sphere. This gave a better approximation for each sphere centre. Because of noise on the data and the relatively coarse accumulator resolution* used (10 mm), it was necessary to perform a further step in order to ensure that the data points used to compute the sphere centre coordinates were reliably chosen.

This additional step was to return to the original data set and extract all points within a small radial tolerance (current radius estimate + 2 mm)† of the current best estimate of each sphere centre. These points were then used to compute a better estimate of the sphere centre coordinates using the same LabVIEW algorithm as previously. The radial residuals of the fit were also calculated and plotted.

In addition, extra processing was required to eliminate any falsely detected spheres by checking the computed radius for each sphere.

The output of this processing step was a list of sphere centre coordinates, one list for those detected in front-face and one for back-face.

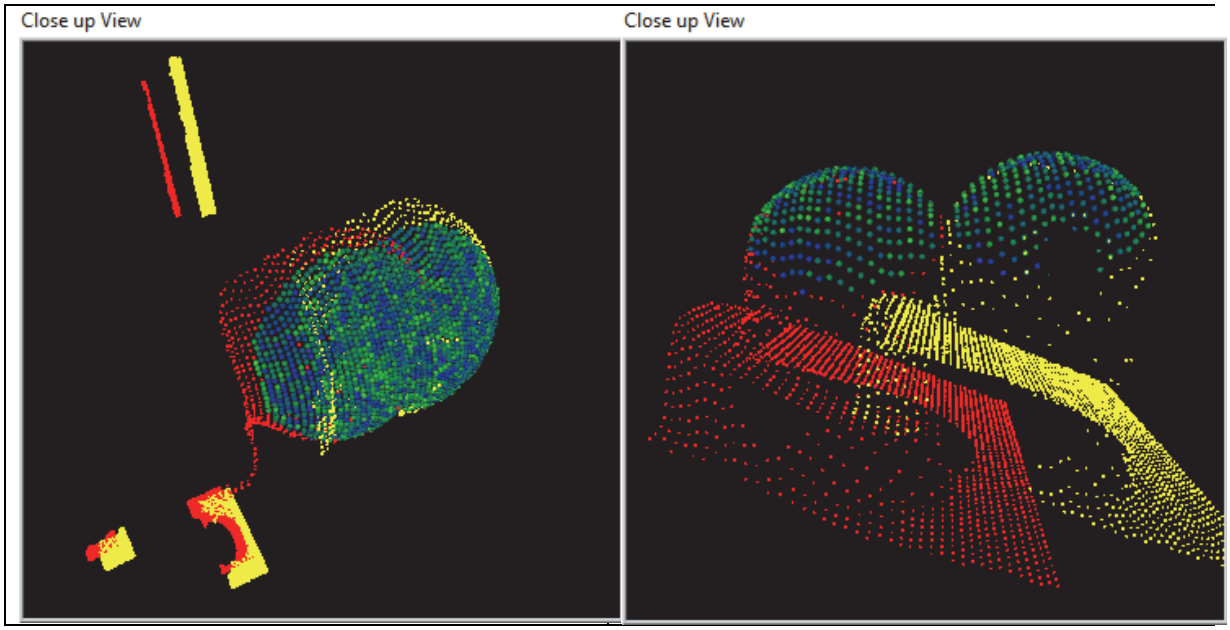

Figure 7 Two examples of the data points used to compute the coordinates of the centre of the sphere. The picture shows two images of the same sphere the red points were scanned in front-face and the yellow points in back-face. The points used to compute the centre of each sphere image are coloured blue/green.

Figure 7 shows examples of areas of the point cloud data around two of the target spheres after the processing described above had been applied. The points scanned in front-face are coloured red and those scanned in back-face are yellow. The two sets of points are distinctly separated. This is due to the un-compensated geometrical errors of the instrument. Note that in the right hand image, the difference

* A smaller accumulator resolution could have been used, but this would significantly increase memory requirements and computing time.
† This tolerance range proved best at ensuring the best selection of data points for the final sphere fit.

between the apparent sphere position determined from the front-face and back-face data is of the order of the sphere diameter, which was 38.1 mm.

4.4 PROCESS SPHERE CENTRE DATA

The sphere centre coordinates were then processed using bespoke software written in Matlab that implemented the process described in Section 3.

5 RESULTS AND OBSERVATION

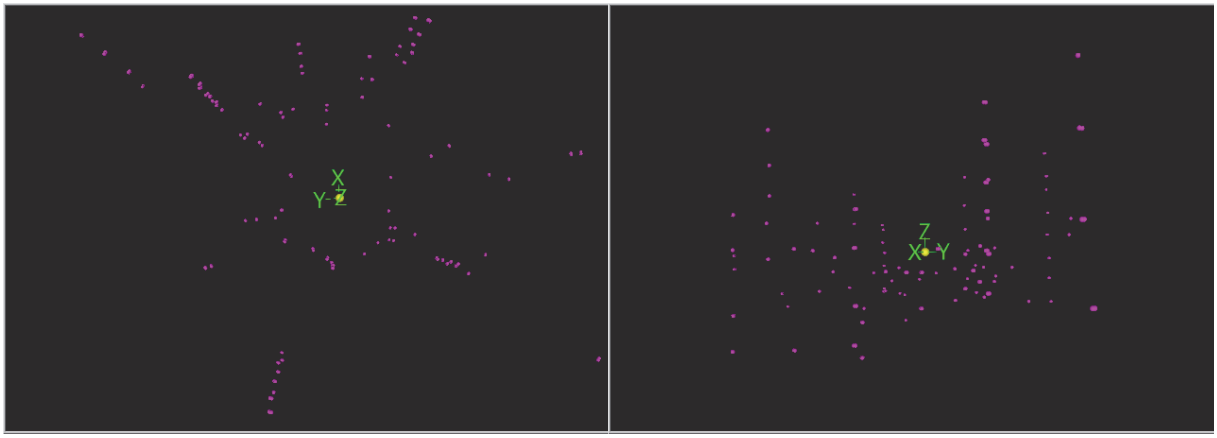

Figure 8 Perspective views from above (left) and the side (right) showing the range (with respect to the scanner) over which data was taken.

Figure 8 shows a combination of all the scans showing the angular and distance range over which data was recorded. The image on the left of Figure 8 shows that data was spread reasonably in horizontal angle with data taken close in and at further distance. The image on the right shows the extent of data in the vertical direction. It was not possible with our setup to locate targets directly above the scanner or at elevation angles higher than 52.7° or lower than -44.2°.

5.1 SPHERE CENTRE LOCATION

The range from the scanner to the target spheres varied from approximately 1299 mm to 6733 mm and the number of points used to compute the centre coordinates varied accordingly between 77 to 2320 points. The range of distances and number of points per target for each of the four scans are shown in Table 2.

Table 2 Scanner-to-target distance range and the range of number of data points per target for the four scans

Scan	Distance to target /mm		Number of points per target	
	Maximum	Minimum	Maximum	Minimum
1	5890	1694	1498	110
2	4824	1299	2320	187
3	4509	1598	1769	102
4	6733	1413	2011	77

All target spheres were therefore well within the operating range of the scanner (0.3 m to 30 m) and the number of data points used to fit the sphere was sufficient. However, due to the line of sight constraints the points are necessarily distributed over a partial sphere as shown in Figure 7.

5.1.1 Sphere radius

The sphere fitting process consistently estimated the sphere radius to be smaller than the nominal radius of 19.05 mm. For example, the estimated radii computed for scan 1 are show in Figure 9 plotted as a function of distance from the scanner. The computed radius varies from just over 18.2 mm to 18.96 mm. There does not appear to be any correlation with range.

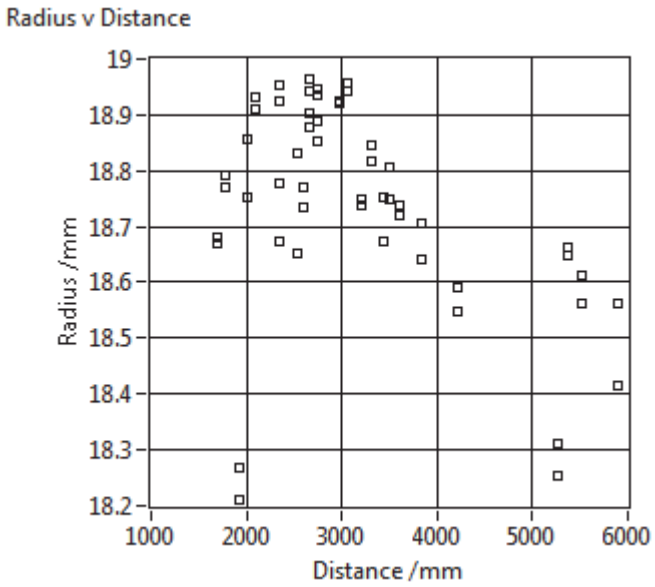

Figure 9 Computed sphere radius versus distance for scan 1.

5.2 MODEL PARAMETERS

Table 3 shows the model parameters and their uncertainties obtained by fitting the model to the sphere centre data obtained from four scans from four different locations. The process was able to estimate all model parameters except for x_{5n} and x_{5z}. This was due to two unresolved degrees of freedom, one involving x_{5z}, x_7 and x_{9z}, and the other involving x_{5n}, and x_{9n}. Examination of the equations on page 2 reveals tight correlation between x_{5z} and x_7, and between x_{5n} and x_{9n}. These correlations can be broken, and the unresolved degrees of freedom resolved if x_{5n} and x_{5z} are fixed by some other means.

Table 3 Model parameters determined by the fit to experimental data.

Parameter	Description	Value /mm or arc seconds	Uncertainty /µm or arc seconds
x_{1n}	Beam offset along N	0.512	23
x_{1z}	Beam offset along Z	-0.136	32
x_2	Transit axis offset	-0.117	7
x_3	Mirror offset	0.520	13
x_4	Vertical index offset	15.025	0.5
x_{5n}	Beam tilt along N	-	-
x_{5z}	Beam tilt along Z	-	-
x_6	Mirror tilt	665.807	0.9
x_7	Transit axis tilt	-173.052	2.4
x_{8x}	Horizontal encoder eccentricity along X	-16.545	0.5
x_{8y}	Horizontal encoder eccentricity along Y	14.342	0.5

x_{9n}	Vertical encoder eccentricity along N	13.067	2
x_{9z}	Vertical encoder eccentricity along Z	1.274	7
x_{10}	Range zero offset	0.817	31
x_{11a}	Horizontal encoder scale error (2^{nd} order)	-2.992	1
x_{11b}	Horizontal encoder scale error (2^{nd} order)	-1.287	0.5
x_{12a}	Vertical encoder scale error (2^{nd} order)	-9.740	6
x_{12b}	Vertical encoder scale error (2^{nd} order)	-9.214	4

5.3 TARGET POSITIONS

Table 4 lists the target sphere centre coordinates and their corresponding uncertainties determined by the fit of the model to the data. These parameter values represent those that would be obtained if the scanner was corrected using the error model described in Section 2 and the model parameters listed in Table 3.

Table 4 Target coordinates obtained from the model fit to the data.

Target coordinates /mm			**Target coordinate uncertainties /µm**		
x	***y***	***z***	**u(*x*)**	**u(*y*)**	**u(*z*)**
-310.1	2284.7	-1073.6	41	50	72
-300.8	1943.5	-367.3	33	37	62
-313.2	1526.3	-668.4	36	36	62
-1195.6	3005.1	669.0	41	41	116
-1203.2	2950.7	313.3	39	41	110
-1705.3	-2320.2	-1031.1	49	41	90
-1674.2	-2328.7	789.6	39	38	104
404.1	-1410.6	-1260.5	42	55	72
806.2	-2387.8	-858.9	40	45	76
860.8	-2400.1	723.2	33	46	66
1573.7	-1335.1	-384.6	34	37	62
2936.0	-1823.4	590.8	41	30	57
2924.2	-1784.6	-98.1	40	30	66
2969.3	-1762.0	2401.1	61	52	91
2948.4	-1739.5	1113.4	45	32	61
2958.2	-1735.2	1705.0	47	32	67
2570.0	-988.2	45.7	34	29	57
2223.3	-745.2	-90.2	29	28	53
1740.6	111.2	-381.2	29	26	53
2154.8	846.4	-386.2	36	26	58
2255.0	1557.7	21.6	36	32	58
1676.6	1950.3	-372.7	33	40	65
3158.9	4250.8	2577.9	63	90	144
3139.2	4260.6	1574.2	54	63	134
3112.8	4237.5	344.3	43	54	121
3091.5	4323.9	-831.6	46	60	126

5.4 RESIDUALS

Table 5 lists the standard deviation of the residuals of the individual sensor data. These values represent the standard uncertainty of the system when compensated using the error model described in Section 2 and the model parameters listed in Table 3.

Table 5 Standard deviation of length and angle residuals.

Sensor	Standard deviation of residuals
Rm	107 µm
Hm	3.8 arc seconds
Vm	7.1 arc seconds

6 SUMMARY AND CONCLUSIONS

An experiment has been carried out to investigate the feasibility of applying the "network test" that has previously been developed at NPL for laser tracker calibration to 3D scanners such as the Surphaser model 25HSX IR-X. A scanner error model developed at NIST has been used for this work.

An experiment was performed using 26 1.5 inch diameter spherical targets scanned from four different locations. All geometric error compensation was disabled. The resulting point clouds were processed to separate data scanned in front-face from that scanned in back-face, and each resulting data sets were further processed to isolate data points on each spherical targets. These data points were then used to compute the centre coordinates of each target.

The sphere centre coordinates were then fitted to a mathematical model of the experimental process that included the error model of the scanner using a non-linear least squares algorithm. This fit yielded the target coordinates, scanner locations and orientations, and the scanner error model parameters and their uncertainties.

The process was able to determine all but two of the scanner error model parameters, but some parameters were tightly correlated and two degrees of freedom were unresolved. The target centre coordinates were located with maximum uncertainties in x, y and z of 63 µm, 90 µm and 144 µm, respectively.

The standard uncertainty in the individual sensors was estimated to be 107 µm for the range sensor and 3.8 arc seconds and 7.1 arc seconds for the horizontal and vertical angle sensors respectively.

The higher uncertainty obtained for the vertical angle sensor and the z axis target coordinates is likely to be due to the lack of targets positioned at the extreme of the elevation range.

6.1 LIMITATIONS OF THE CURRENT METHOD

The following limitation applied or were observed during this work.

1. The sphere radius was consistently determined by the software to be smaller than the nominal radius. The reason for this could be, for example, insufficient coverage of the surface, or a distortion effect due to the finite size of the laser beam spot and its distortion when projected onto the sphere surface.
2. There was no up-to-date calibration of the ranger system, and no calibrated scale in the setup.
3. The range linearity behaviour observed by NIST is not explained by the model, and no therefore taken into account in the data processing.
4. There were no targets directly above or at very high elevation angles, which could improve the angle encoder calibration.

6.2 FUTURE POSSIBILITIES

The following improvements to this experiment could be made by NPL in a follow-up project.

1. Include ranger errors in the model and optimise the network to allow the range errors to be identified in the calibration process.
2. Introduce scale either using a reference artefact or a laser tracker to ensure traceability to the metre.
3. Use larger spheres to reduce distortion of the laser spot when projected onto the surface and/or compensate for spot distortion and its effect on the range measurement.
4. Investigate the unresolved degrees of freedom and correlations and a method of resolving them.

REFERENCES

1 E Baumann, F R Giorgetta, J-D Descenes, W C Swann, I Coddington and N R Newbury, "Comb-calibrated laser ranging for three-dimensional surface profiling with micrometer-level precision at a distance", *Optics Express* **22** (1) 24914-28, 2014.

2 M Ferrucci, B Muralikrishnan, D Sawyer, S Phillips, P Petrov, Y Yakovlev, A Astrelin, S Milligan and J Palmateer, "Evaluation of a laser scanner for large volume coordinate metrology: a comparison of results before and after factory calibration", *Meas. Sci. Technol*. **25** , 105010, 2014.

3 M Ferrucci, B Muralikrishnan, C Blackburn, D Sawyer, S Phillips, V Lee, P Petrov,Y Yakovlev, A Astrelin, S Milligan, J Palmateer, "Ranging performance evaluation of a laser scanner", Proceedings of the 28th Annual, Meeting of the ASPE 2013, St. Paul, MN, USA.

4 B Hughes, W Sun, A Forbes, A Lewis, "Determining laser tracker alignment errors using a network measurement", Journal of the CMSC, **5** (2) 26-32, 2010.

5 B Hughes, A Forbes, A Lewis, W Sun, D Veal and K Nasr, "Laser tracker error determination using a network measurement", *Meas. Sci. Technol.* **22** (4) 045103 (2011).

6 M Ferrucci, B Muralikrishnan, C Blackburn, D Sawyer, S Phillips, V Lee, P Petrov, Y Yakovlev, A Astrelin, S Milligan, J Palmateer, "Performance evaluation of a laser scanner", LVMC 2013, Manchester, UK.

7 B Muralikrishnan, M Ferrucci, D Sawyer, G Gerner, V Lee, C Blackburn, S Phillips, P Petrov, Y Yakovlev, A Astrelin, S Milligan and J Palmateer, "Volumetric performance evaluation of a laser scanner", Proceedings of the 28th Annual Meeting of the ASPE 2013, St. Paul, MN, USA.

8 B Muralikrishnan, M Ferrucci, D Sawyer, G Gerner, V Lee, C Blackburn, S Phillips, P Petrov, Y Yakovlev, A Astrelin, S Milligan and J Palmateer, "Volumetric performance evaluation of a laser scanner", 2014, *Prec. Eng*. **40** 139–150, 2015.